Examination of the shock wave regular reflexion phenomenon in a rarefied supersonic plasma flow

S. Mazouffre,[a] V. Caubet-Hilloutou, and J. C. Lengrand
Laboratoire d'Aérothermique, 1C avenue de la Recherche Scientifique, 45071 Orléans, France

E. Pawelec
University of Opole, Oleska 48, Opole, Poland

The flow properties of a low-pressure weakly ionized supersonic argon plasma jet are examined using Fabry–Pérot interferometry and laser induced fluorescence spectroscopy. The flow velocity and equilibrium temperature measured at the torch nozzle exit are in close agreement with computational fluid dynamics calculations. The model also predicts the plasma flow to be in a rarefied regime. Departure from thermal equilibrium is indeed observed behind the nozzle where the parallel temperature differs significantly from the perpendicular temperature. The development of the axial velocity component along the jet center stream line reveals the occurrence of the shock wave regular reflexion phenomenon: No Mach disk is formed and the flow experiences successive supersonic-to-supersonic transitions before reaching a subsonic regime. Shock wave regular reflexion is in fact favored under our experimental conditions since the speed ratio is high and the rarefaction degree is pronounced at the nozzle exit. © *2005 American Institute of Physics*. [DOI: 10.1063/1.1835345]

I. INTRODUCTION

From a technological point of view, low-pressure supersonic plasma flows are currently employed for thin film deposition, microstructure etching, surface passivation, and treatment of archaeological artifacts.[1,2] All these applications are based on an optimal energy conversion from the plasma source to the gases used for surface modification or treatment and they take advantage of the high flow velocity in terms of processing duration. Supersonic plasma jets also find applications in the field of aerospace engineering where they serve as simulation tools for some of the specific conditions encountered during high speed flights in planetary atmospheres. At present, plasma jets are employed to investigate hypersonic plane flights in the upper layers of the Earth's atmosphere[3] and entry of a space probe into the Mars' atmosphere.[4] Knowledge about the properties of the plasma that is created in front of the vehicle for a given atmosphere composition and a given trajectory is necessary for instance for optimization of the vehicle's thermal shield,[3] for determination of the plasma frequency, which drives attenuation in radio transmissions,[5] and to investigate plasma enhanced lure and camouflage effects. Wind tunnels equipped with dc arc torch and capable of producing continuous rarefied plasma jets offer two advantages over other ground-based simulation means like shock tubes and pulsed wind tunnels: The easiness of probing the jet owing to its large size, and stationary flow conditions for several hours with a low level of contamination. Whereas numerous laser-aided experiments have been performed to study the plasma flow dynamics and chemistry in the field of plasma processing,[6–9] only few works have been devoted to the investigation of the flow structure of jets used in the field of aerospace by means of nonintrusive techniques.[10,11] However, in the latter case one can expect very specific flow features. To investigate supersonic plasma flow characteristics around a body necessitates the use of large scale plasma jets produced thanks to the expansion of a thermal plasma through a large convergent-divergent nozzle. As a consequence, the velocity is high and the rarefaction degree is pronounced at the nozzle exhaust. Under such conditions, it is likely that the shock wave regular reflexion phenomenon occurs: The downstream supersonic-to-subsonic transition occurs smoothly by way of the formation of several expansion cells without the presence of a Mach disk. In order to correctly simulate a vehicle trajectory through upper layers of an atmosphere, it is obvious that the plasma jet properties, in terms of flow velocity, must be well identified especially as a complex shock wave pattern does exist.

In this contribution, we report on laser induced fluorescence and Fabry–Pérot interferometry measurements on argon atoms in a low-pressure supersonic plasma flow generated from argon gas seeded with a small amount of molecular nitrogen. Such an experiment can be considered as a test case, in the sense that the absence of a complex chemistry, with respect to N_2-O_2 and CO_2 plasmas, makes easier the understanding of the observed phenomena. From the measurements, macroscopic flow parameters like axial and radial velocity components and temperature of neutral argon atoms are extracted both inside the nozzle and in the free plasma jet. It will be shown that the downstream supersonic-to-subsonic transition is governed by regular reflexion. Furthermore, the appearance of a peculiar flow structure in the vicinity of the nozzle lip is reported and discussed.

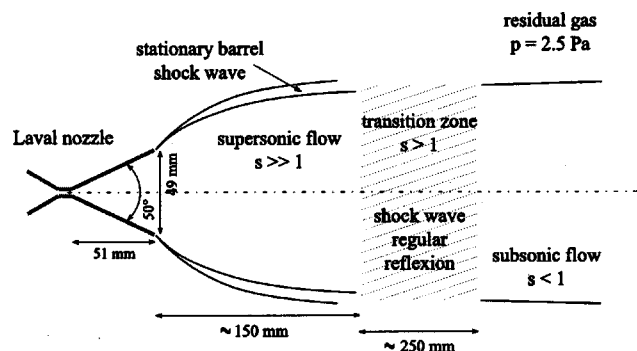[a]Author to whom correspondence should be addressed. Electronic mail: mazouffre@cnrs-orleans.fr

FIG. 1. Drawing of the convergent-divergent nozzle and sketch of the free jet expansion. Under our conditions, the transition between the supersonic flow regime and the subsonic flow regime occurs without the formation of Mach disks.

II. PLASMA SOURCE AND PLASMA FLOW FEATURES

The plasma source used in the ground-test facility, the so-called SR5 wind tunnel, is a water-cooled vortex stabilized dc-arc torch.[12] The torch is equipped with a tungsten cathode and with a convergent (60°)-divergent (50°) copper nozzle that acts as a grounded anode. The length of the divergent part is 5.1 cm and the exit diameter of the nozzle is 4.9 cm, see Fig. 1. The arc extends from the tip of the cathode through a 4 mm diameter molybdenum throat and attaches diffusely to the nozzle. The plasma torch can be operated in a wide range of currents (10 to 300 A) and flows (5 to 50 slm), and it can be run for several hours, the lifetime being determined by the cathode erosion. Gases are fed through mass flow controllers directly into the cathode area. The torch is mounted on an arm that can be moved in vertical and horizontal directions.

A thermal plasma is created in argon gas seeded with a small amount of molecular nitrogen for experimental convenience (see Sec. IV). Subsequently the plasma expands from the torch nozzle into a low pressure steel vessel. The vacuum chamber is 4.3 m long and has a diameter of 1.1 m. The pumping system is made of three large Roots blower pumps evacuated by a set of roughing pump. The capacity of the pump stack is 26 000 $m^3 h^{-1}$, which ensures a residual pressure down to 1 Pa during operation. Standard operating conditions for this experiment are summarized in Table I. The cathode to anode gap is 1 mm. The efficiency is around 65% and the specific enthalpy is 10.5 kJ g^{-1}. The two quantities are estimated from the consumed electrical power, the latter

TABLE I. Standard operating conditions.

Parameter	Value
I	100 A
U	45 V
$\dot{m}_{Ar}$	0.26 g s^{-1}
$\dot{m}_{N_2}$	0.04 g s^{-1}
p_{torch}	76 kPa
$p_{chamber}$	2.5 Pa

TABLE II. On-axis conditions at the nozzle exhaust under our experimental conditions. The electron density profile has been previously reported (Ref. 12). λ refers to the local mean free path for momentum exchange.

Parameter	Value	Means
n_{Ar}	2×10^{21} m^{-3}	Calculation
λ_{Ar-Ar}	8 mm	Calculation
n_e	$\approx 10^{18}$ m^{-3}	Langmuir probe
T_{eq}	2440 K	LIF
v_z	4.7 km s^{-1}	LIF
h	11.0 kJ g^{-1}	Calculation

being deduced from the torch cooling water temperature. Typical sizes of a jet produced in the SR5 wind-tunnel are 0.2 m in diameter and about 1 m in length.

A detailed description of the physics of rarefied supersonic plasma jets is available elsewhere.[13,14] As the plasma expands through a convergent-divergent nozzle from a high pressure region into a low pressure region, a well-defined free jet shock wave structure is produced, as shown in Fig. 1. The plasma first flows supersonically: The Mach number reaches 1 at the nozzle throat and the flow is supersonic in the divergent portion. In this flow domain, the temperature drops and the drift velocity increases due to energy conservation. In the mean time, the particle density along a streamline decreases because of the increase in the jet diameter. In case of an underexpanded jet, the flow domain is limited by a barrel shock wave behind the nozzle exit. At some distance from the source, depending among others upon the background pressure, the side shock waves interact with one another on the jet axis. Depending upon the exit Mach number and the rarefaction degree, two shock wave configurations are then possible as explained by Graur and co-workers.[15] A Mach disk associated with an oblique reflected shock can be created through which the flow undergoes a supersonic to subsonic transition: Mach reflection. Under specific conditions, i.e., large Mach number and high level of rarefaction, the Mach disk vanishes and the flow experiences a supersonic-to-supersonic transition with a slight decrease in the Mach number magnitude: Regular reflection. The latter process can occur several times over appreciable distances leading to the appearance of several stationary expansion cells. The transition between regular and Mach reflexion of shock waves in steady gas flow has been extensively studied.[16,17] Beyond the overall shock region, the plasma flows subsonically at constant static pressure. Deviation from the classical free jet flow picture may appear in the case of transient species like radicals and charged particles.[6,18,19]

The value of some flow parameters under standard operating conditions are given in Table II at the torch nozzle exhaust.[20] As can be seen, the ionization degree α is very low ($\alpha < 10^{-3}$) and the flow is in a transition regime. The low ionization degree is due to the addition of a small amount of molecular nitrogen (see Sec. IV). The specific enthalpy calculated from the obtained velocity and temperature is in close agreement with the measured one, showing that measurements warrant energy conservation in the course of the flow.
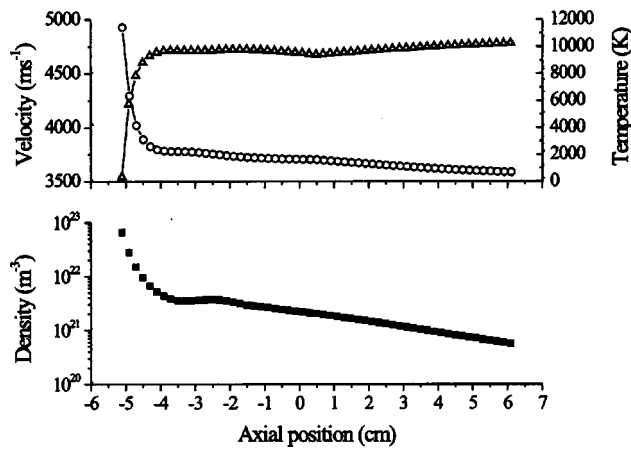
FIG. 2. Top: Calculated development of the Ar atom flow velocity (triangle) and translational temperature (circle) along the symmetry axis. Bottom: Calculated axial Ar atom density profile. The position $z=0$ corresponds to the nozzle exit plane.

Calculations have been carried out to determine the flow properties inside the nozzle as well as in the first centimeters of the jet with a method based on continuum fluid mechanics developed by Broc *et al.* described in Ref. 21. Calculations start at the nozzle throat. Conditions upstream of the throat are determined from the measured enthalpy and mass flow rate: One finds $T=17\,600$ K and $p=3.1\times10^4$ Pa. In the divergent part of the nozzle, the flow is treated as an axisymmetric viscous expansion using parabolized Navier–Stokes equations. The code accounts for velocity slip and temperature jump at the wall. Downstream of the nozzle exhaust viscous effects are neglected, besides, the background pressure is set to zero, which prevents from predicting the formation of shock waves beyond the nozzle. In the model, we assume that the gas is solely composed of argon atoms, i.e., the presence of ions and electrons is neglected. For the transport coefficients, however, we take into account the effect of ionization.[22] Such an assumption, which has already been applied in the case of an argon plasma jet, is valid, since it was revealed that the dynamic properties of a weakly ionized plasma expansion are governed by the heavy particles.[6,23]

The calculated on-axis velocity and temperature profiles are shown in Fig. 2. The flow accelerates and cools down abruptly behind the nozzle throat. Inside the diverging portion the velocity does not vary much whereas it slightly increases behind the exhaust. Accordingly, the temperature continually decreases, first in a fast manner over a short distance and then slowly. The calculated Ar atom density profile along the axis is displayed in Fig. 2. The density drops behind the throat is due to flux conservation. The stationary density plateau inside the nozzle is a direct consequence of the abrupt angle change between the throat and the divergent section. Note the corresponding anomaly in both the velocity and temperature profiles 3 cm ahead of the exit plane. The macroscopic flow parameters at the nozzle exit are $v_z=4690$ m s^{-1}, $T=1650$ K, and $n=2.1\times10^{21}$ m^{-3}. The relevant rarefaction parameter in a supersonic flow is the so-called Bird's parameter P defined as

$$P = \frac{1}{n\langle\sigma v_r\rangle} \times \frac{v_z}{\ell}, \tag{1}$$

where n is the density of the collision partner, σ is the collision cross-section, v_r is the relative speed, v_z is the particle flow velocity, and ℓ is the density gradient scale length. Value of the cross section for momentum exchange are taken from the work of Phelps.[24] At the nozzle exit, ℓ is equal to 61.8 mm. Therefore, the dimensionless Bird's parameter is equal to 0.09, which is larger than the critical value 0.02, meaning that departure from equilibrium between the perpendicular and the parallel temperature must be expected.

III. OPTICAL DIAGNOSTIC TOOLS

A. Fabry–Pérot interferometry

The complete Fabry–Pérot (FP) interferometry bench has been extensively described in a previous paper.[12] The light emanating from the plasma is collected with a lens and transported toward the optical bench by means of a multimode optical fiber. A similar fiber is also used to carry part of the light emitted by a low pressure argon lamp, which is used as a reference for null velocity. The two optical fibers are then combined into one. Subsequently, the light leaving the fiber coupler is collected with a lens in such a way that a collimated beam of light is created. The parallel beam passes a plane Fabry–Pérot cavity. Behind the cavity, the transmitted light is focused onto a pinhole in order to solely select the central interference ring. A monochromator acts as a rough wavelength selector to separate the line to be studied from the remainder of the spectrum. A photomultiplier tube (PMT) is used as a light detector. The free spectral range of the cavity is equal to 9.924 GHz. In the wavelength region of interest, the FP setup allows to achieve a spectral resolution of 0.15 GHz.

Two configurations of the photon collection branch are available: The line of sight is oriented either at 90° or at 60° with respect to the jet symmetry axis. With the first configuration, one can measure the perpendicular temperature $T_\perp$ associated with the velocity distribution perpendicular to a stream line. Using the second configuration, one obtains the axial velocity component, after correction with the cosine of the angle, as well as the parallel temperature $T_\parallel$. Note that such a configuration allows to probe the plasma flow inside the nozzle. The long field depth of the observation branch, around 25 cm in our case, forbids to achieve a good spatial resolution. Thus, the obtained line profile corresponds to the one averaged along the line of sight, which prevents from measuring the radial velocity component.[12]

Two Ar line profiles are analyzed with the Fabry–Pérot setup. The Ar I line at 763.51 nm and the Ar I line at 738.40 nm. These two Ar lines offer several advantages: They are well isolated, they both correspond to a relatively strong transition, and the PMT quantum efficiency is relatively high below 800 nm. The temperature is deduced from the Doppler broadening of the line taking into account the apparatus width. The Doppler shift of the observed line allows to determine the mean velocity in the direction of observation.
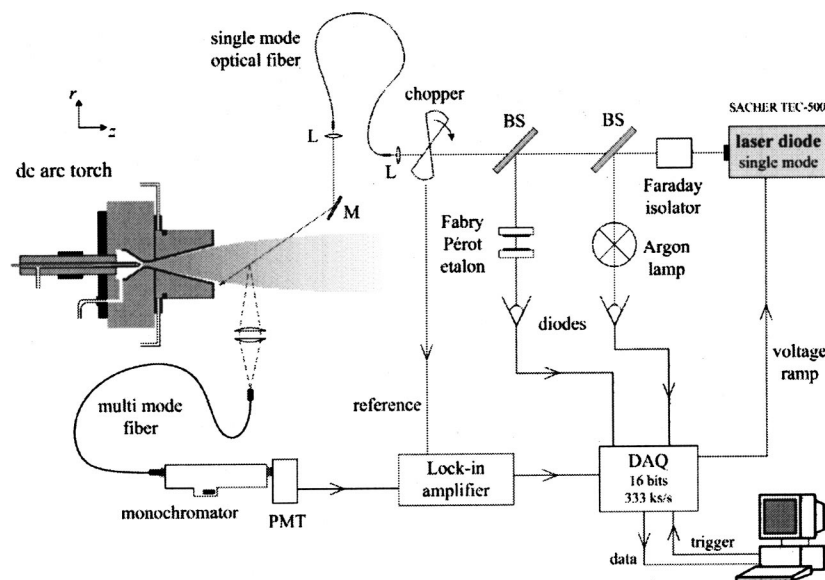
FIG. 3. Schematic view of the experimental cw-LIF setup using a single mode tunable laser diode and phase sensitive detection. The laser beam can be directed either perpendicular or obliquely (at an angle of 30°) with respect to the flow direction. The map of the plasma plume properties is realized by moving the arcjet.

B. Laser induced fluorescence

A schematic of the laser induced fluorescence (LIF) optical bench is depicted in Fig. 3. A single mode tunable external cavity diode laser (SACHER TEC 500 in Littman configuration) delivers 3 mW of horizontally polarized near-infrared radiation (800 to 830 nm) with a bandwidth of 1 MHz. A Faraday isolator prevents any reflected beam of light to enter back into the laser cavity. A small fraction of the beam is passed through a low-pressure argon lamp. The absorption spectrum measured in that way is used to define the unshifted frequency position. A second beam splitter directs a small part of the laser into a 3.3 GHz Fabry–Pérot etalon to monitor mode structure and to ensure that no mode hop occurs during operation. The mode-hop free tuning range of the laser is typically 30 GHz with voltage-current coupling. The recorded transmission of the Fabry–Pérot etalon is also used to linearize the frequency axis. The laser beam is coupled into a single mode optical fiber with a 5 μm core diameter using a 4 mm focal distance lens. Such a device allows us to obtain a 30% coupling efficiency without shaping the beam. Two excitation configurations are possible. In one configuration using a plane gold mirror located inside the vacuum chamber, the laser beam propagates opposite to the plasma flow direction at a 30° angle with respect to the jet axis. In another configuration the beam is directed perpendicular to the flow direction. In both cases a 4 mm focal distance lens is used to focus the beam leaving the optical fiber onto the axis. The beam diameter is estimated to be around 2 mm in the probed zone.

The laser light is chopped at a frequency of about 750 Hz and the laser induced fluorescence signal is detected on a horizontal axis normal to both excitation directions. The signal is collected with two lenses ($f_1 = 100$ cm and $f_2 = 20$ cm) and imaged onto the entrance side of a 1 mm core diameter multimode optical fiber. The fiber is connected to a 20 cm focal distance monochromator centered at 810 nm with a bandwidth of about 0.5 Å in order to filter out extraneous plasma light. The 1 mm aperture of the fiber positioned at the focal plane of the imaging lens system determines the spatial resolution. The magnification is equal to 4, hence the resolution in horizontal direction is 4 mm. Phase-sensitive detection is used to discriminate the fluorescence light from the intrinsic plasma emission which is about 1000 times greater. The signal delivered by the PMT is analyzed with a lock-in amplifier which is synchronized to the chopper frequency. The current integration time of the lock-in amplifier is 300 ms. All signals are recorded simultaneously with a 16 bits 333 kHz analog-to-digital converter (National Instruments PCI-6052E). The scanning of the laser frequency is controlled by supplying a low voltage to the piezoelectric block connected to the end mirror of the laser diode cavity. Typical scan times are several minutes. Complementary information about determination of atom velocity by means of continuous-wave LIF spectroscopy can be found in references.[9,25]

All LIF measurements presented in this contribution correspond to excitation of the Ar[$1s_4$] resonant level. The laser frequency is scanned over the $1s_4 \rightarrow 2p_7$ transition at 810.37 nm. Four fluorescence waveforms obtained with the LIF diagnostic tool after axial excitation are shown in Fig. 4. Also shown in this figure is the absorption spectrum in a low pressure Ar lamp, which is used as a reference for determining the zero Doppler shift. Note that the laser power varies during a scan over the Ar transition, therefore LIF profiles must be corrected in order to obtain the proper baseline.

The bandwidth of the laser is in the order of 10 MHz, much narrower than the width of the measured Ar profiles. Both Stark broadening and pressure broadening can be neglected in view of, respectively, the low electron density and the low gas pressure.[26] Furthermore, the saturation parameter S is found to be 0.03 for the concerned transition.[27] Since S is much less than unity, the transition is not saturated meaning that the deposited laser power has no influence upon the Ar line shape. Hence, a recorded spectral profile is a direct measurement of the local Ar atom velocity distribution function, or in other words, of the local Ar atom energy distribu-
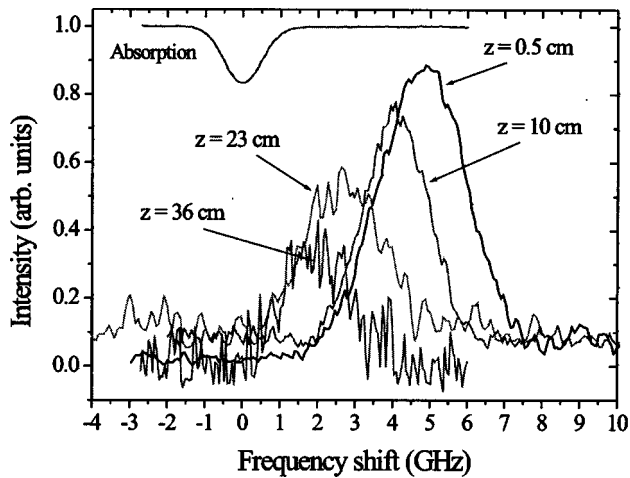
FIG. 4. Axial velocity profiles obtained with the LIF diagnostic tool after excitation of the $Ar[1s_4]$ state for several axial locations z. Also shown is the absorption spectrum in a low pressure Ar lamp, which serves as a Doppler shift reference.
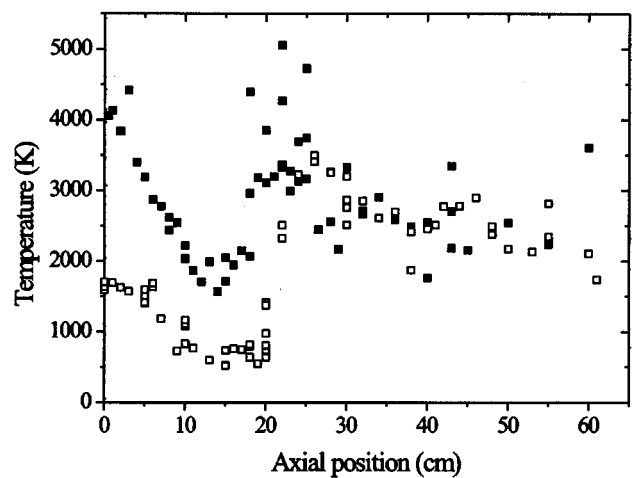

FIG. 5. On-axis profile of the perpendicular temperature $T_\perp$ (open square) and the parallel temperature $T_\parallel$ (full square). Two compression stages are observed at $z \approx 20$ cm (strong) and at $z \approx 45$ cm (weak), respectively.

tion function. The mean Ar atom velocity is deduced from position of the fluorescence peak relative to the line measured in the argon lamp and the temperature is related to the width of the measured profile. As can be seen in Fig. 4, the shape of the Ar atoms velocity distribution function does not change in the course of the expansion, however, the mean velocity and the velocity spread, i.e., the thermal speed, depend upon the location in the jet.

IV. INTERPRETATION OF MEASURED SPECTRA

In view of the low electron temperature behind the nozzle exit, which is in the order of the heavy particle temperature,[6] light emitted by the plasma jet mostly originates in the radiative deexcitation of Ar atom excited states formed in a three particle recombination process involving Ar ions

$$Ar^+ + e + e \rightarrow Ar* + e. \qquad (2)$$

Therefore, the flow properties of the probed excited Ar* atoms image in first instance the behavior of Ar^+ ions. Note that it is well known that all Ar* atoms produced in this way cascade down to the $4s$ multiplet.[9] However, it has been shown that in case of an argon plasma expansion, the behavior of Ar^+ ions is linked to the behavior of Ar atoms.[9] In other words, monitoring the Ar* atoms properties is an indirect way of determining the properties of Ar atoms, i.e., an indirect way of obtaining the plasma flow properties since ground-state Ar atoms are the major species in the jet. A detailed explanation of the Ar^+-Ar coupling in a low-pressure plasma jet can be found in Ref. 9. Here we briefly summarize the main ideas. Behind the nozzle exit, friction between Ar^+ ions and Ar atoms is large enough to insure a fully mixed flow via transfer of momentum. Indeed, calculations reveal that the Ar^+-Ar collision length λ_{Ar^+-Ar} is around 0.1 mm and λ_{Ar-Ar} is equal to 8 mm.[24] The two mean free paths are very small in comparison with the density gradient scale length ($\ell = 61.8$ mm) and with the nozzle exhaust diameter ($d = 48$ mm). One should also consider the existence

of a local electric field generated from gradients in charge density. However, the resulting acceleration of Ar ions can be neglected in view of the electron density profile which warrants a very low electric field magnitude.[12] A last effect is also of importance, especially in the case of LIF measurements. Under our experimental conditions, due to the VUV radiation trapping, both resonant and ground states of the argon atom are efficiently coupled and can therefore be considered as being fully mixed.[9] Combining all these effects, one establishes that the velocity distribution of resonant $Ar[1s_4]$ atoms and ground-state Ar atoms are identical.

The addition of a small fraction of molecular nitrogen simply permits to limit both the emission and the reabsorption of infrared light. It has no influence upon the overall plasma flow characteristics. The efficient charge exchange reaction between Ar atoms and N_2^+ ions

$$Ar^+ + N_2 \rightarrow Ar + N_2^+, \qquad (3)$$

leads to the disappearance of a large number of Ar^+ ions, which are at the origin of the existence of Ar* atoms as aforementioned. According to reference,[28] the addition of 10% of N_2 to an argon plasma leads to a drop of the electron density of more than one order of magnitude, that explains the low measured ionization degree under our conditions (see Table II). Reaction (3) is followed by the fast dissociative recombination of the formed N_2^+ molecular ion.[28]

V. STANDING SHOCK WAVES

A. Evidence of the compression effect

The development along the jet centerline of the perpendicular temperature $T_\perp$, associated with the distribution function of the Ar atom radial velocity component—with respect to the jet axis—is shown in Fig. 5. Note that $z=0$ corresponds to the nozzle exit. The temperature first decreases due to the supersonic expansion of the plasma jet. The observed abrupt rise of $T_\perp$ indicates the presence of a diffuse stationary shock wave that stretches from $z=15$ cm to $z=25$ cm, through which kinetic energy is converted into thermal en-

ergy. Behind the shock front, the temperature decreases due to the formation of a steady expansion cell. A secondary compression zone is located around $z = 45$ cm, as confirmed by velocity measurements. Far downstream, where the flow gets subsonic, the temperature decreases slowly due to energy exchange with the residual ambient gas and heat transfer to walls.

The axial profile of the parallel temperature $T_\parallel$, associated with the distribution function of the Ar atom axial velocity component, is also shown in Fig. 5. The shape of the $T_\parallel$ profile resemble the one of $T_\perp$ and they are both directly connected to the jet shock wave structure. Across the shock front, the parallel temperature rises up to 5000 K. Behind the domain of high shock strength, the two temperatures are in equilibrium with of a value around 3000 K. As can be seen in Fig. 5, the gap between $T_\parallel$ and $T_\perp$ is about 2500 K at the nozzle exit. A departure from thermal equilibrium, which is a direct consequence of the rarefaction effect, was expected in view of the Bird's parameter value. At a certain position inside the divergent section of the nozzle the number of collisions becomes too low to maintain equilibrium between the two temperatures that quickly diverge from each other as the expansion process proceeds with $T_\perp < T_\parallel$ as explained by Miller and Andres.[29] At the outlet, the equilibrium temperature T_{eq} obtained from $T_\perp$ and $T_\parallel$ is higher than the calculated temperature T: $T_{eq} = 2440$ K and $T = 1650$ K. The discrepancy may originate from the arc voltage fast oscillations.[30] Fluctuations of the voltage lead to fluctuations of the atom drift velocity via changes in enthalpy. As soon as the measurement time scale is much longer than any characteristic oscillation time, velocity fluctuations are then responsible for an artificial broadening of the distribution function. As an example, fluctuations of 5% in voltage under our conditions lead to a fluctuation of 3% in velocity, that means a temperature overestimate of a few percents. As can be observed in Fig. 5, the temperature gradients along the jet centerline markedly differ depending on the temperature of interest. Furthermore, and surprisingly, the magnitude of gradients is contrary to expectations. The theory predicts that $\nabla T_\parallel < \nabla T_\perp$ in axial direction in agreement with previously reported experimental outcomes obtained with a supersonic nitrogen plasma jet.[19] This observed phenomenon is not yet understood.

B. Shock wave regular reflexion

The evolution of the axial velocity component v_z along the jet centerline is shown in Fig. 6. Also shown in this figure is the local thermal velocity calculated from the parallel temperature $T_\parallel$. The most probable thermal speed reads

$$v_{th} = \sqrt{\frac{2k_B T_\parallel}{m}}, \tag{4}$$

where k_B is the Boltzmann constant, and m is the mass of the species. Contrary to the speed of sound, the thermal speed does not depend on the specific heat ratio γ, which is always difficult to estimate in case of a plasma generated from a mixture between an atomic gas and a molecular gas. The two approaches anyway give similar results. Note that throughout
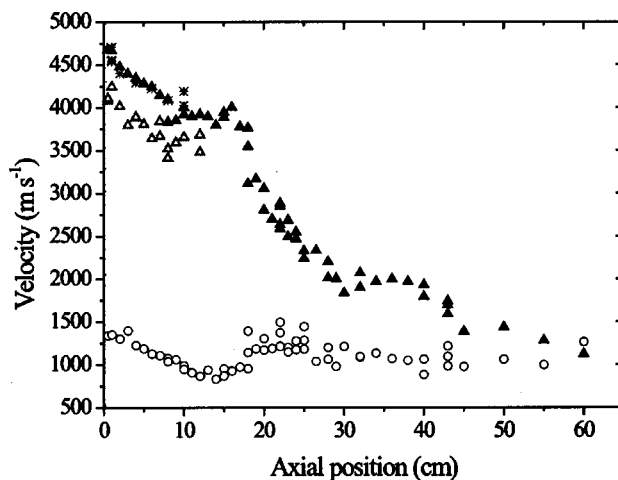

FIG. 6. Evolution of the profile of the axial velocity component (triangle) along the jet centerline. The open triangle symbols correspond to experimental values of v_z obtained with a fresh cathode. The star symbols correspond to measurements performed with a 0.065 g s^{-1}N$_2$ mass flow rate. Also shown is the thermal speed calculated from the measured parallel temperature (circle). The supersonic to subsonic transition occurs at $z \approx 60$ cm.

the remainder of the paper, the molecular speed ratio

$$s = \frac{v_z}{v_{th}}, \tag{5}$$

has been used rather than the Mach number.

The on-axis velocity profile displayed in Fig. 6 reveals the existence of several stationary shock waves that find their origin in the regular reflexion phenomenon: No Mach disk is formed and the flow undergoes a supersonic to supersonic transition across the shock wave with a speed ratio reduction.[15–17] Two of such standing shock waves are visible in Fig. 6 at $z \approx 15$ cm and $z \approx 40$ cm, respectively. Throughout a standing shock wave the flow experiences a deceleration through a positive pressure gradient that originates in a compression effect. Across the first shock front, the speed ratio drops from 4.7 to 1.8. Across the second shock front, the speed ratio decreases from 1.8 to 1.5. In both cases, the flow stays supersonic behind the shock wave, which is the signature for regular reflexion. The zone between two consecutive shock waves, through which the temperature decreases, are referred to as expansion cell. As can be seen in Fig. 6, the plasma flow becomes subsonic around $z = 60$ cm.

The regular reflexion phenomenon is favored under our experimental conditions according to numerical calculations carried out by Graur to investigate transition conditions between Mach and regular reflexion of shock wave in underexpanded jets in terms of speed ratio s (or Mach number) and Bird's parameter P (or Knudsen number).[15] By varying the nozzle exit conditions in terms of s and P, Graur and coworkers evidence different regimes for the structure of the shock wave that limit the first expansion cell. Note that their calculations were based on a variant of Navier–Stokes equations.[15] The regular reflexion phenomenon occurs when, in the nozzle exit section, both s and P are large. Under our conditions, at the nozzle exit the speed ratio is rather high with a value of 3.6 and the rarefaction effect is already pro-

nounced since $P=0.09$. The present situation can be compared with previous experiments performed on underexpanded argon plasma jet at the University of Eindhoven by Engeln *et al.*[9] In the latter situation, a straight nozzle was employed and the flow parameters at the exhaust were the following: $s=1$ (sonic orifice) and $P\approx 10^{-3}$. A Mach disk was found to be created through which the plasma flow did undergo a supersonic to subsonic transition, as predicted by Graur *et al.*[15]

As can be seen in Fig. 6, the on-axis Ar atom velocity v_z decreases from 4.7 km s^{-1} down to 3.9 km s^{-1} in the first ten centimeters of the free expansion domain. In the meantime, the thermal speed drops from 1.3 km s^{-1} down to 0.9 km s^{-1}. Consequently the speed ratio increases from 3.6 to 4.3. The measured magnitude of the axial velocity at the nozzle exit is in close agreement with the calculated value. However, calculation does not predict a large drop of the velocity behind the nozzle. In order to cancel out any experimental artifact, a measurement series has been realized with a higher molecular nitrogen flow.[31] It appeared to be necessary to check whether the decrease in velocity observed at the torch outlet was not connected to a modification of the Ar atom velocity distribution function. Indeed, reabsorbtion of fluorescence light by slow atoms located along the observation path and the subsequent change in the velocity distribution may be erroneously interpreted as a decrease in the local average drift velocity. As can be seen in Fig. 6, the experiment clearly demonstrates that the observed trend is real. Notice that the added amount of N$_2$ is not large enough to lead to a global decrease in the velocity magnitude. Similarly, the parallel temperature is not affected by a small change in the N$_2$ contents.[31]

A first suggestion is that the observed decrease in velocity behind the nozzle exit is the consequence of either the existence of a complex shock wave reflexion phenomenon, like an oblique standing shock wave attached to the lip of the nozzle,[32] or a high plasma flow viscosity. As can be seen in Fig. 2, the fluid model shows that at the nozzle exit the axial velocity falls down by an amount of 50 m s^{-1} while the translational temperature decreases by an amount of 200 K due to viscosity. The measured deceleration is nevertheless stronger since the velocity decreases by an amount of 500 m s^{-1} and the equilibrium temperature falls from 2240 to 1460 K from $z=0$ to $z=10$ cm, respectively. Another idea is that the measured drop is a consequence of a slight misalignment of the laser beam with respect to the jet centerline. Liebeskind *et al.* employed such an argument to explain a decrease in velocity measured behind a nozzle in the case of a supersonic hydrogen arc jet plume.[25] In our case, numerous series of measurements have been performed with different flows and different cathode states, as shown in Fig. 6, and a realignment of the laser beam and the detection branch in between two series has always been done. Notwithstanding the realignement procedure, the trend has always been observed.[31] The presence of an oblique shock wave is unlikely at low background pressure, hence the velocity drop is certainly driven by viscosity. However, a more elaborated model, which for instance could account for the residual
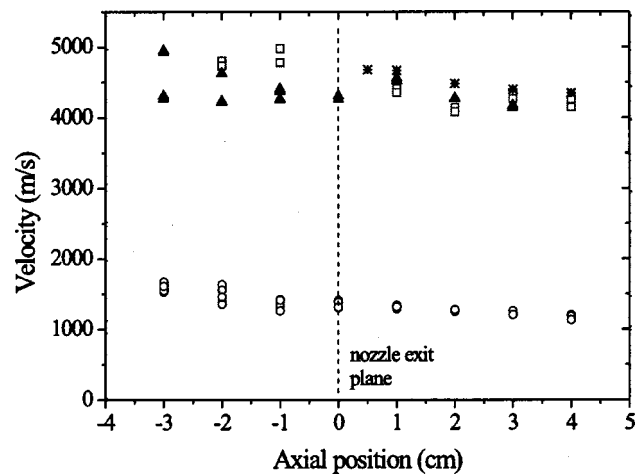

FIG. 7. On-axis profile of the axial velocity component measured by interferometry with the 738 nm (full triangle) and 763 nm (open triangle) Ar lines. Also shown is the thermal speed calculated using the measured temperature (circle) as well as the velocity measured by LIF (star). $s\approx 3.3$ at the nozzle exit.

background gas, is needed to be able to accurately calculate flow structures, and to confirm that the observed structure is a real flow characteristic.

VI. PLASMA FLOW INSIDE THE NOZZLE

As can be seen in Fig. 7, measurements of the development of the axial velocity along the jet axis have also been carried out by means of Fabry–Pérot interferometry inside the nozzle as well as at the nozzle exhaust.[12] The velocity magnitude is in relative good agreement with the one measured by LIF. Despite the poor spatial resolution of the Fabry–Pérot setup one can observe the drop in velocity behind the nozzle. A speed ratio of 3.3 is found at the nozzle outlet. The Ar atom flow velocity is nearly constant in the divergent part of the nozzle with a value of about 4.5 km s^{-1} in good agreement with numerical outcomes. It experimentally proves that the acceleration of the plasma flows and the corresponding cooling occur right behind the nozzle throat.

The radial development of the Ar atom axial velocity component has been measured inside the arcjet nozzle at $z=-2$ cm by means of Fabry–Pérot interferometry. The corresponding profile is shown in Fig. 8. As expected, the velocity is maximum on axis and the profile is almost symmetric. The axial velocity approaches the thermal speed in the vicinity of the nozzle wall.

VII. JET RADIAL STRUCTURE

A. At the nozzle exit

Both the parallel temperature and the axial velocity component have been measured by means of LIF at the nozzle exit ($z=0$ cm) as a function of the radial position r. The obtained profiles are displayed in Fig. 9. The velocity profile exhibits a bell curve shape with a maximum velocity magnitude on the jet axis.[33] The plasma flow is supersonic in the jet core and it becomes sonic, i.e., $s=1$, at $r\approx 2.5$ cm ($v_{th}=650$ m s^{-1} with $T=1000$ K), a position that corresponds to
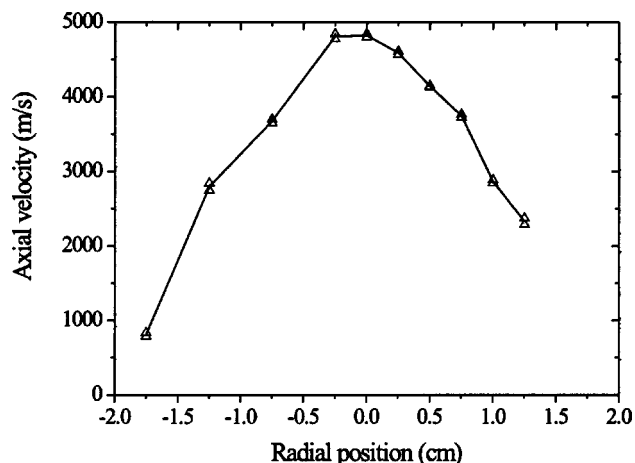
FIG. 8. Radial profile of the axial velocity component measured by interferometry with the 738 nm Ar line inside the nozzle ($z=-2$ cm). As expected, the velocity is maximum on axis and it approaches the thermal speed close to the wall of the torch nozzle.

FIG. 10. Radial and axial Ar atom velocities combined to form a radial profile of the velocity vector 10 cm from the nozzle exit plane. The jet boundary, which is defined as the location where $v=0$, is located at $r=10$ cm. The corresponding expansion half-angle is 33°.

the nozzle surface boundary. There is no clear structure in the parallel temperature profile inside the core of the jet. The temperature outside the jet, i.e., in front of the metal torch housing, is around 800 and 1200 K for, respectively, $r<0$ and $r>0$. An interesting feature is visible in Fig. 9 at the radial location that corresponds to the nozzle lip and more or less to the sonic limit. The velocity is suddenly negative with a magnitude of about 3 km s^{-1} while the temperature abruptly drops to 300 K. The observed feature is certainly a sign for the existence of a specific well-localized structure such as recirculation cells surrounding the plasma jet. The rotation speed of a vortex can lead to the measurement of a negative Doppler shift. Moreover, the magnitude of the as-
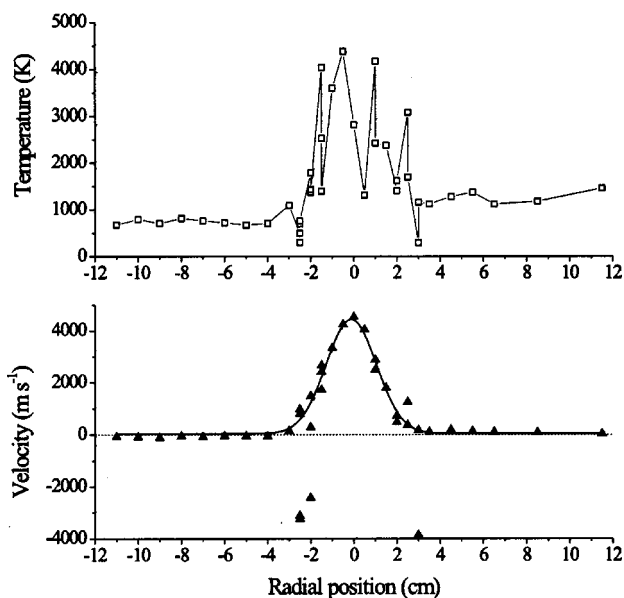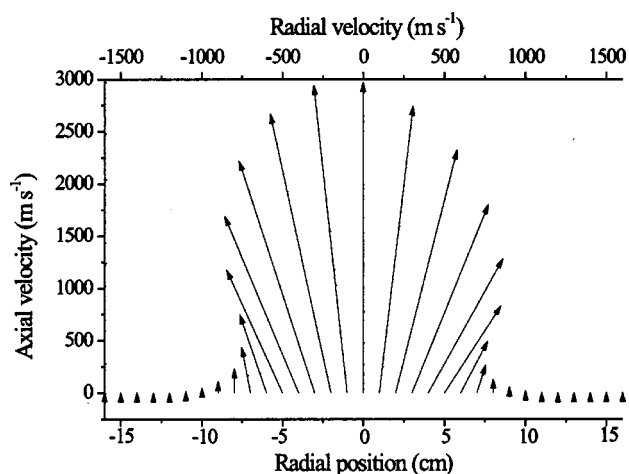
sociated velocity can be high due to gas entrainment. Nevertheless, the existence of such a stable cell can hardly explain the observed low gas temperature.

B. In the plume

The radial and axial Ar atom velocity components measured 10 cm away from the nozzle exit plane have been combined to form a radial profile of the velocity vector. The resulting vector plot is shown in Fig. 10. The profile is almost symmetrical with a maximum velocity on axis. The jet boundary, which is defined as the location where $v_z=0$, is located at $r=10$ cm. The corresponding expansion half-angle is 33°. It is then higher than the nozzle half-angle that is equal to 25° meaning that the jet opens behind the nozzle exhaust. The temperature on axis is around 1700 K and the temperature beyond the jet boundary, i.e., in the background gas is 500 K.[31] The radial velocity is null on the jet centerline and it reaches its maximum value (600 m s^{-1}) at $r=3$ cm.[12] As can be seen in Fig. 10, the radial velocity returns back to zero at $|r|=8$ cm. It implies that from $r=8$ cm to $r=10$ cm the flow velocity is parallel to the jet center stream line, which is a feature of a barrel shock wave.

VIII. CONCLUSION

Flow properties of an underexpanding weakly ionized argon plasma jet seeded with a small amount of nitrogen have been investigated applying Fabry–Pérot interferometry and laser induced fluorescence techniques on resonant Ar atom excited states. A detailed examination of atomic collision processes and radiation transport under our plasma conditions clearly establishes that the local velocity distribution function of Ar resonant states images the velocity distribution of ground-state argon atoms. Measurements reveal that both the speed ratio and the rarefaction degree are high at the torch nozzle exit. As a consequence, the plasma deceleration process, which originates in the interaction between the plasma jet and the residual background gas, is found to be

FIG. 9. Radial profile of both the parallel temperature (top) and the axial velocity component (bottom) measured at the nozzle exhaust ($z=0$ cm). The solid line is drawn to guide the eye.

governed by the regular reflexion phenomenon. The supersonic-to-subsonic transition necessitates several stages in the course of which the Ar atom flow velocity gradually decreases. Strong departure from thermal equilibrium is observed behind the nozzle outlet as the result of rarefaction. Finally, experimental results point out the presence of a stable flow structure in the vicinity of the nozzle lip. In this narrow cell, of which the existence still must be confirmed, the gas is relatively cold and the flow velocity is opposite to the jet velocity.

An obvious continuation of works described in this contribution is the investigation of a rarefied supersonic argon plasma flow around an obstacle of various geometry and material. To monitor argon ions and argon neutrals behavior throughout bow shock waves as well as in boundary layers would fournish with valuable information about plasma-body interactions. This might open the way in the near future toward active plasma control features by playing with the supersonic vehicle wall properties.

ACKNOWLEDGMENTS

[1] J. W. A. M. Gielen, W. M. M. Kessels, MCM. van de Sanden, and D. C. Schram, J. Appl. Phys. **82**, 2643 (1997).

[2] R. Engeln, S. Mazouffre, P. Vankan, I. Bakker, and D. C. Schram, Plasma Sources Sci. Technol. **11**, A100 (2002).

[3] G. S. R. Sarma, in *Molecular Physics and Hypersonic Flows*, edited by M. Capitelli (NATO ASI Series, Kluwer Academic Publishers, Boston, 1995), p. 1.

[4] D. Paterna, R. Monti, and R. Savino, J. Spacecr. Rockets **39**, 227 (2002).

[5] P. Bletzinger and B. N. Ganguly, *Proceedings of the 8th AIAA International Space Planes and Hypersonic Systems and Technologies Conference, Norfolk* (AIAA, 1998), AIAA paper 98-1572.

[6] M. C. M. van de Sanden, R. van der Bercken, and D. C. Schram, Plasma Sources Sci. Technol. **3**, 501 (1994).

[7] R. F. G. Meulenbroeks, R. A. H. Engeln, J. A. M. van der Mullen, and D. C. Schram, Phys. Rev. E **49**, 4397 (1994).

[8] S. Mazouffre, M. G. H. Boogaarts, I. S. J. Bakker, P. Vankan, R. Engeln, and D. C. Schram, Phys. Rev. E **64**, 016411 (2001).

[9] R. Engeln, S. Mazouffre, P. Vankan, D. C. Schram, and N. Sadeghi, Plasma Sources Sci. Technol. **10**, 595 (2001).

[10] A. Del Vecchio, G. Palumbo, U. Koch, and A. Gülhan, J. Thermophys. Heat Transfer **14**, 216 (2000).

[11] A. K. Mohamed, B. Rosier, P. Sagnier, D. Henry, Y. Louvet, and D. Bize, Aerospace Sci. Technol. **4**, 241 (1998).

[12] S. Mazouffre, E. Pawelec, V. Caubet-Hilloutou, and M. Dudeck, *Proceedings of the 34th AIAA Plasmadynamics and Lasers Conference, Orlando* (AIAA, 2003), AIAA paper 03-3747. Both the Ar and N_2 gas flow cited in the AIAA paper are erroneous due to a bad calibration of the mass flow controllers. The correct values are the ones mentioned in the present article.

[13] D. R. Miller, in *Atomic and Molecular Beam Methods*, edited by G. Scoles (Oxford University, New York, 1988), p. 14.

[14] D. C. Schram, S. Mazouffre, R. Engeln, and M. C. M. van de Sanden, in *Atomic and Molecular Beams*, edited by R. Campargue (Springer, New York, 2001), p. 209.

[15] I. A. Graur, J. C. Lengrand, and T. G. Elizarova, *Proceedings of the 22nd International Symposium on Shock Waves, London*, edited by G. J. Ball, R. Hiller, and G. T. Roberts (Imperial College, London, 2000), Vol. 2, p. 1267.

[16] M. S. Ivanov, G. N. Markelov, A. N. Kudryavtsev, and S. F. Gimelshein, AIAA J. **36**, 2079 (1998).

[17] M. S. Ivanov, D. Vandromme, V. M. Fomin, A. N. Kudryavtsev, A. Hadjadj, and D. V. Khotyanovsky, Shock Waves **11**, 199 (2001).

[18] S. Mazouffre, M. G. H. Boogaarts, J. A. M. van der Mullen, and D. C. Schram, Phys. Rev. Lett. **84**, 2622 (2000).

[19] S. Mazouffre, I. Bakker, R. Engeln, P. Vankan, and D. C. Schram, Plasma Sources Sci. Technol. **11**, 439 (2002).

[20] The equilibrium temperature T_{eq} is given by $\frac{3}{2}kT_{eq} = kT_\perp + \frac{1}{2}kT_\parallel$, where k is the Boltzmann constant. The specific enthalpy h is calculated as follows: $h = (C_p/M)T_{eq} + v_z^2/2$, where C_p is the specific heat and M is the molar weight.

[21] A. Broc, S. De Benedictis, G. Dilecce, M. Vigliotti, R. G. Sharafutdinov, and P. A. Skovorodko, J. Fluid Mech. **500**, 211 (2004).

[22] M. I. Boulos, P. Fauchais, and E. Pfender, *Thermal Plasmas, Fundamentals and Applications* (Plenum Press, New York, 1994), Vol. 1, p. 355.

[23] S. E. Selezneva, M. I. Boulos, M. C. M. van de Sanden, R. Engeln, and D. C. Schram, J. Phys. D **35**, 1362 (2002).

[24] A. V. Phelps, J. Appl. Phys. **76**, 747 (1994).

[25] J. G. Liebeskind, R. K. Hanson, and M. A. Cappelli, Appl. Opt. **32**, 6117 (1993).

[26] D. Schinköth, M. Kock, and E. Schulz-Gulde, J. Quant. Spectrosc. Radiat. Transf. **64**, 635 (2000).

[27] W. Demtröder, *Laser Spectroscopy* (Springer, Berlin, 1998), p. 432.

[28] G. J. H. Brussaard, M. C. M. van de Sanden, and D. C. Schram, Phys. Plasmas **4**, 3077 (1997).

[29] D. R. Miller and R. P Andres, in *Proceedings of the 6th Rarefied Gas Dynamics Symposium, Cambridge*, edited by L. Trilling and H. Y. Wachman (Academic Press, New York, 1969), Vol. 2, p. 1385.

[30] V. Lago, M. de Graaf, and M. Dudeck, High Temp. Mater. Processes **1**, 179 (1997).

[31] S. Mazouffre, V. Caubet-Hilloutou, M. Dudeck, and E. Pawelec, in *Proceedings of the 1st International Workshop on Radiation of High Temperature Gases in Atmospheric Entry, Lisbon*, edited by B. Warmbein (ESA Publications Division, Noordwijk, 2003), Proceedings SP 533, p. 47.

[32] A. S. Stern, P. C. Waterman, and T. F. Sinclair, J. Chem. Phys. **33**, 805 (1960).

[33] A. H. M. Habets, Ph.D. thesis, Eindhoven University of Technology, the Netherlands (1977).